

Probabilistic effect of metastable excitation on lock-in amplified plasma laser-induced fluorescence diagnostics at modulation frequencies comparable to the fluorescence frequency

Di Jiang¹, Chen-yao Jin^{1,2}, Chi-Shung Yip^{1,†}, Wei Zhang^{1,†}, Guo-Sheng Xu¹ and Liang Wang¹

¹Institute of Plasma Physics, Hefei Institutes of Physical Science, Chinese Academy of Sciences, Hefei 230031, PR China

²University of Science and Technology of China, Hefei 230026, PR China

(Received 25 January 2022; revised 26 April 2022; accepted 27 April 2022)

In this paper, effects of discharge parameters and modulation frequency on the signal of laser-induced fluorescence measurements of ion velocity distribution functions are investigated in the LIF Test Source. A maximum modulation frequency is found for each given set of parameters, beyond which the signal gradually declines. Meanwhile, this maximum modulation frequency occurred consistently at $\sim 1/10$ of the theoretical frequency limit and photon counts received by a photomultiplier tube, which indicates that as modulation frequency and the associated per-pulse-excitation-event count decrease, the transition from the macroscopic statistical signal to the microscopic probabilistic signal is a gradual process.

Key words: plasma diagnostics, plasma properties

1. Introduction

Laser-induced fluorescence (LIF) of metastable ions is a non-invasive, direct measurement of the ion velocity distribution function (Yip & Jiang 2021). With more than 30 years of development, laser-induced fluorescence is becoming an increasingly common plasma diagnostics tool for measuring the velocity distribution functions of ions and neutral particles in studies of Hall thrusters (Mazouffre *et al.* 2008; Mazouffre 2012; Duan *et al.* 2020), linear devices (Boivin & Scime 2003; Keesee, Scime & Boivin 2004; Sun *et al.* 2005), plasma processing (Zimmerman, McWilliams & Edrich 2005; Jacobs *et al.* 2007; Moore, Gekelman & Pribyl 2016), and basic plasma physics (Lee *et al.* 2006; Lee, Hershkowitz & Severn 2007a; Lee, Oksuz & Hershkowitz 2007b; Yip, Hershkowitz & Severn 2010; Yip *et al.* 2016). As an optical diagnostic, atomic excitation is the basic process of light emission. In single-photon LIF, a laser of known

† Email addresses for correspondence: csyip@ipp.ac.cn, zhangwei@ipp.ac.cn

wavelength excites an electron transition in a metastable ion or neutral to an excited state, then its fluorescence is detected as a signal when the electron relaxes to the low-energy state. Due to the small excitation energy available from diode lasers, single-photon LIF diagnosis usually detects metastable ions or neutrals rather than ground-state ones. With the development of hardware, such as high-sensitivity photomultiplier tubes (PMTs), high-frequency lock-in amplifiers and high-frequency choppers, we can conduct a series of high-frequency experiments. For example, Romadanov *et al.* (2018) attempted time-resolved LIF measurements to study breathing mode in Hall thrusters. However, one cannot achieve better time resolution than the photon count rate, unless the coherence time of the phenomena multiplied by the photon count rate is significant. Therefore, this work studies the signal evolution when the modulation frequency is close to the fluorescence frequency which refers to the limit frequency of fluorescent photons produced by laser photons under given plasma discharge parameters that can be calculated by the collision radiation model (CRM) or the fluorescence counting frequency determined by the gain of a PMT.

2. Collision radiation model

In low-temperature plasmas, metastable ions are often generated by a single ionization event with high-energy electrons (Chu, Hood & Skiff 2019). For example, in argon plasmas, this is expected to occur due to the following reaction:



The signal intensity measured by LIF can be estimated by the CRM (Wilson *et al.* 1995; Barnat & Weatherford 2015; Chu *et al.* 2017; Chu & Skiff 2018), which estimates the generation and excitation rates of collision frequencies that produce metastable ions. These frequencies are given by the general collision model:

$$S_{ij} = n_i n_e \int_{-\infty}^{\infty} \sigma_{ij}(E) v_e(E) f_e(E) dE = \langle n_i n_e \sigma_{ij}(E) v_e(E) \rangle. \quad (2.2)$$

In this model, S_{ij} denotes the rate at which the collision process excites ions or neutral particles from state i to state j , $\sigma_{ij}(E)$ and $v_e(E)$ are the energy distribution of the collisional cross-section and the electron velocity when transition at electron energy E , respectively, and $f_e(E)$ is the electron energy distribution. Through the collision model, the rate of metastable production can be estimated by the electron collision excitation process: $\langle n_{meta} n_e \sigma_{excite}(E) v_e(E) \rangle$. Here n_{meta} , the density of metastable ions, can in turn be estimated by balancing the loss rate with the production rate: $\langle n_{n,g} n_e \sigma_{nm}(E) v_e(E) \rangle + \langle n_{i,g} n_e \sigma_{im}(E) v_e(E) \rangle$, each of these terms representing production of metastable ions from ground-state neutrals and ions by electron collisions.

The process of metastable excitation by a laser can be similarly treated as a photon-ion collision event, and the energy distribution of photons can be well approximated as a group of single-velocity particles incident at a photon flux Γ_{photon} . Thus the equation of this collision event can be simplified as $n_i \sigma_{ij} \Gamma_{photon}$ (Wilson *et al.* 1995). Flux Γ_{photon} can be determined by the laser injection power and wavelength.

According to this model, both laser photon collision excitation and electron collision excitation are summarized to obtain the rate at which metastable ions are excited to the excited state. In addition, metastable quenching rate S_{quench} should also be included. Consequently, the excitation rate of the metastable ions given a metastable density n_{meta}

can be written as

$$S_{ex} = \langle n_{meta} n_e \sigma_{excite}(E) v_e(E) \rangle + n_{meta} \sigma_{LIF} \Gamma_{photon} + S_{quench}, \quad (2.3)$$

where $\langle n_{meta} n_e \sigma_{excite}(E) v_e(E) \rangle$ is the electron collision excitation rate and $S_{quench} = \langle n_{meta} n_n \sigma_{quench}(E) v_i(E) \rangle$ is the rate of collisional quenching caused by metastable collisions with background particles. Note that only a portion of the laser excitation rate $n_{meta} \sigma_{LIF} \Gamma_{photon}$ results in LIF signal, determined by the branching ratio of the transitions from the excited state to the different relaxed state.

The CRM is generally adapted to describe the physical processes behind plasma LIF diagnostics and could be considered a statistical model. Particularly with experiments employing continuous-wave lasers, this is at least in part due to the adaption of a low laser modulation frequency much lower than the fluorescence frequency, whether technologically limited or deliberately chosen by design (Wang & Hershkowitz 2006; Yip *et al.* 2010, 2016). As the modulation frequency increases, the probabilistic aspect of the excitation process also becomes significant and will affect the resultant LIF signal. This work presents experimental investigation of such effects.

3. Probabilistic model and its effects on lock-in amplification

The fundamental physical model behind the CRM is that whether a photon excites a metastable is by nature probabilistic and the associated probability of excitation depends on the cross-section in question. The resultant photon count calculated from the CRM is therefore a statistically expected value. Provided a large number of events per observation, i.e. a sufficiently large number of photons streaming through a sufficient amount of metastables in the diagnosed space per modulated laser pulse, the resultant signal strength per pulse will be close to this expected value. However, as the number of expected excitation events per modulated pulse decreases, the number of probabilistic events within a pulse is no longer sufficient to form a statistical result. Rather, the total number of a large number of modulated pulses reflects the expected number of excitation events, i.e. fluorescent photons, per pulse. This transition from statistical to probabilistic signal can occur via metastable density, laser power and modulated pulse width reduction. The underlying mathematical process calculating the statistically and probabilistically expected signal strength is one and the same, but the probabilistic nature of this expected value is revealed as the number of events per pulse reduces. Thus, the physical picture of the CRM can be both statistical and probabilistic.

Here we revisit the working principles of lock-in amplification to examine how the microscopic probabilistic fluorescence affects signal retrieval. A phase-sensitive detector (PSD) is equivalent to a bandpass filter with extremely narrow bandwidth. The basic module includes a multiplication module for multiplying the input signal and the reference signal and a filter module effectively defining the integration time within which the multiplied signal is time-averaged.

Signal $S_I(t)$ is defined as a time-frequency input signal mixed with noise, and $S_R(t)$ is a reference signal with a fixed frequency relationship with the input signal to be measured. A signal with known modulation entering the PSD module can be defined as $S_I(t) = A_I \sin(\omega t + \varphi) + B(t)$, where ω is the modulation frequency and $B(t)$ is the total noise. The standard reference input to the signal channel is given as $S_{R0}(t) = A_R \sin(\omega_0 t + \theta)$. After the two signals are input into the PSD module for multiplication at the same time,

the output signal obtained is

$$\begin{aligned} S_{PSDO} &= S_I(t)S_{R0}(t) = A_I A_R \sin(\omega t + \varphi) \sin(\omega_0 t + \theta) + B(t)A_R \sin(\omega_0 t + \theta) \\ &= 0.5A_I A_R \cos[(\omega - \omega_0)t + \varphi - \theta] - 0.5A_I A_R \cos[(\omega + \omega_0)t + \varphi + \theta] \quad (3.1) \\ &\quad + B(t)A_R \sin(\omega_0 t + \theta). \end{aligned}$$

When the test signal frequency and the reference frequency are not decoupled, it is usually assumed that $\omega = \omega_0$, that is, the frequencies of the reference signal and the modulated real signal are equal. At this time, the standard signal output by the reference signal channel is $S_R(t) = A_R \sin(\omega t + \theta)$. Therefore, the output signal is $S_{PSDO} = S_I(t)S_R(t) = 0.5A_I A_R \cos(\varphi - \theta) - 0.5A_I A_R \cos(2\omega + \varphi - \theta) + B(t)A_R \sin(\omega t + \theta)$. If the modulated frequency of the input signal equals that of the reference signal, the amplitude of the signal to be measured, i.e. the intensity of the fluorescence signal in this experiment, can be extracted through the first item. The DC part can be obtained by passing the result into a low-pass filter, $S_{output} = 0.5A_I A_R \cos(\varphi - \theta)$.

Figure 1(a,b) shows a schematic diagram of the event counts of metastable excitation and therefore fluorescence. The histogram is the total number of fluorescent photons that can be excited within the period of each pulse, which is a square wave with a duty cycle of 50%. Ideally, the signal strength of each laser is equivalent to the excitation rate discussed in the previous section, giving constant real signal strength over each laser pulse. However, each laser excitation is in fact a probabilistic event. When the excitation frequency is much higher than the modulation frequency, the total photon collection count is essentially a manifestation of a macroscopic collection of excitation events, becoming very close to its statistically expected signal strength as described by the collisional excitation model. On the other hand, as we increase the modulation frequency and therefore reduce the temporal pulse width, the expected number of excitation events within a pulse reduces and eventually becomes totally probabilistic as the expected number of collected photons in each laser pulse becomes close to 1. That is, not every laser pulse produces a photon to be collected, and, within some, more than one photon will be collected. This probabilistic property of the microscopic fluorescence excitation process causes the real frequency of the fluorescent signal to be decoupled from the modulation frequency. Therefore, the output signal is treated by the PSD as noise and averages to 0. Fluorescent signal decoupled and eliminated by the PSD is represented as grey, and from figure 1(a) one can see that the fluorescent signal can be totally discarded by lock-in amplification. On the other hand, the transition from the macroscopic, statistically determined signal to the microscopic, probabilistic signal might not be a sharp one. There might exist a regime such that probabilistic effects manifest, but signal remains retrievable as the proportional variation total collectible photon count per laser pulse in most pulses remains within a relatively small range. This is illustrated in figure 1(b) using an expected photon count of 10 as an example. Due to the probabilistic nature of metastable excitation, not every laser pulse results in the expected photon count, but the proportion of random variation may not be so severe such that an $\omega = \omega_0$ baseline signal can still be strictly retrieved, although the random fluctuations are very likely to be discarded by lock-in amplification. As the modulation frequency decreases and pulse width increases, the collected photon count within a pulse converges to the statistically expected value, thus becoming almost totally retrievable by lock-in amplification. On the other hand, the collected photon count per laser pulse is not only limited by the fluorescence frequency but also by the solid angle which decides the proportion of excited photons being collected, and note that the direction of flight of each individual photon produced in an excitation event is also probabilistically determined.

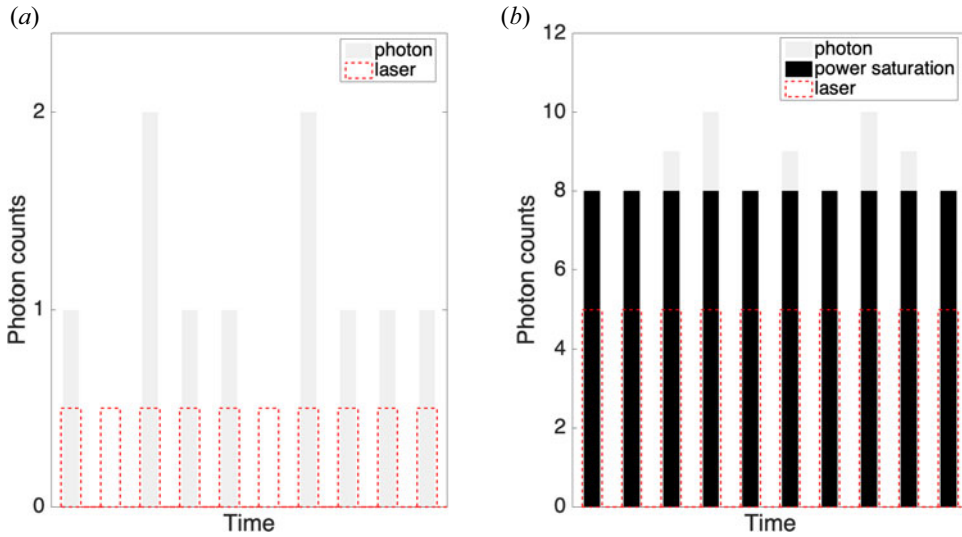


FIGURE 1. Schematic diagram of micro-process in which a metastable state can be excited to produce photons under laser input. (a) Single-photon case. (b) Multi-photon case.

4. Experimental set-up

Experiments are carried out in ASIPP's LIF Test Source (LTS), a multi-dipole confined hot cathode source. A schematic of LTS is shown in figure 2. The chamber is 40 cm long and 20 cm in diameter. Singly ionized argon plasma is produced by electron-impact ionization where primary electrons are emitted by a 2 mm diameter hot LaB₆ cathode. Multi-dipole confinement is realized by 16 rows of magnets with alternating polarities. These magnets are arranged around the periphery of the plasma. On the surface of the magnet, the magnetic field is 1600 G. In the measurement area, the magnetic field is rapidly reduced to less than 2 G. The cathode bias in this experiment is -140 V, which combines with the plasma potential V_p to give the primary electron energy. A mass flow controller is used to maintain a constant neutral gas inflow, thereby maintaining a constant neutral pressure in the chamber. The background pressure of the device is approximately 10^{-5} Pa, and the operating pressure ranges from 10^{-2} to 10^{-1} Pa. A Langmuir probe made with an 11 mm diameter tantalum disc is used to measure the electron density n_e and the electron temperature T_e . Typical plasma parameters for our experiments are $T_e \sim 4$ eV, $n_e \sim 10^9$ cm⁻³.

Our study adopted a three-level Ar II scheme in which a diode laser at a wavelength of 668.614 nm (in vacuum) excites the $3d^4F_{7/2}$ argon ion metastable state to the $4p^4D_{5/2}$ energy level, first proposed by Severn, Edrich & Mcwilliams (1998). The fluorescence radiation from $4p^4D_{5/2}$ to $4s^4P_{3/2}$ has a wavelength of 442.72 nm (in vacuum). A schematic of the LIF optical set-up is shown in figure 3. The black solid lines and the black dotted lines represent the mirrors and laser beam splitters, respectively. A Wavicle ECDL 668 nm Littrow cavity diode laser is used, amplified with a Wavicle TA 668 nm tapered amplifier. The system has been configured to obtain a mode-hop-free tuning range of 100 GHz. In this study, only a small proportion of the tuning range is used, a tuning range of < 15 GHz employed with a laser power change of less than 3%. The laser is modulated via an acoustic optical modulator (AOM), which diffracts the beam periodically when a modulation is applied, splitting the laser beam. The modulation signal generated by

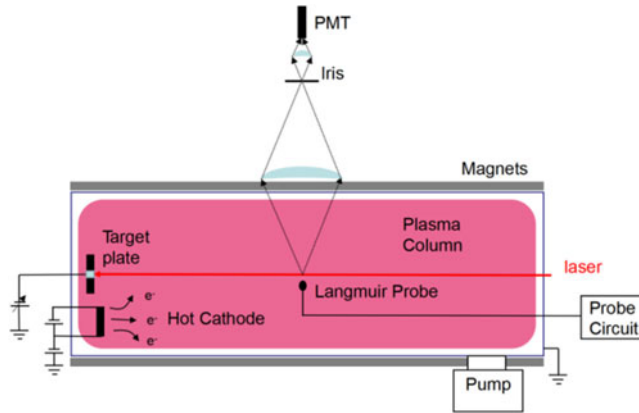


FIGURE 2. Schematic of the LTS multi-dipole chamber.

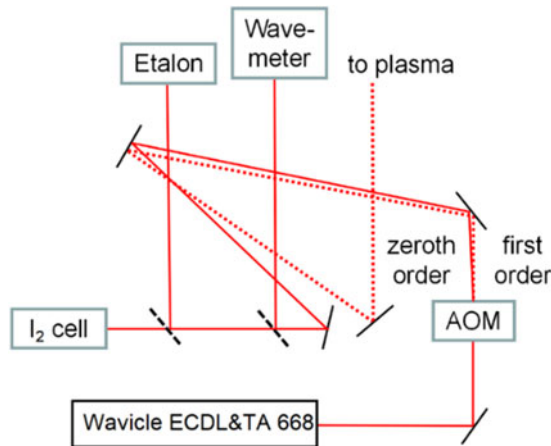


FIGURE 3. LIF experimental set-up.

the AOM is a square wave and the duty cycle is 50%. The zeroth-order beam (the red solid line shown in figure 2), which was incompletely modulated, is directed into a set of wavelength/frequency measurements which are not modulation-sensitive. This beam is 1/10 split twice before being directed into an iodine cell enclosed in a ceramic housing (Keesee *et al.* 2004; Severn, Lee & Hershkovitz 2007) used for absolute wavelength calibration. A 1/10 split beam is directed into a Fabry–Pérot etalon with a free spectrum range of 1.5 GHz and a finesse of 200 (Cooper & Laurendeau 1997). Another 1/10 split beam is directed into a HiFinesse WS-5 wavelength meter for online monitoring of mode-hop-free tuning. The first-order diffraction (the red dotted line shown in figure 2), which is completely modulated, is injected into the chamber through an optical fibre coupling, and then injected into the plasma. The Ar II fluorescent radiation is collected by a PMT at 90° relative to the axis of the laser beam shown in figure 1. The type of PMT is a Hamamatsu H19492-003 with a load resistance of 50 Ω. The control voltage is measured at 0.562 V and the gain is 10⁴. A SYSU OE 2031 DSP lock-in amplifier is used to recover the LIF signal from the ambient background noise. The laser scanning time

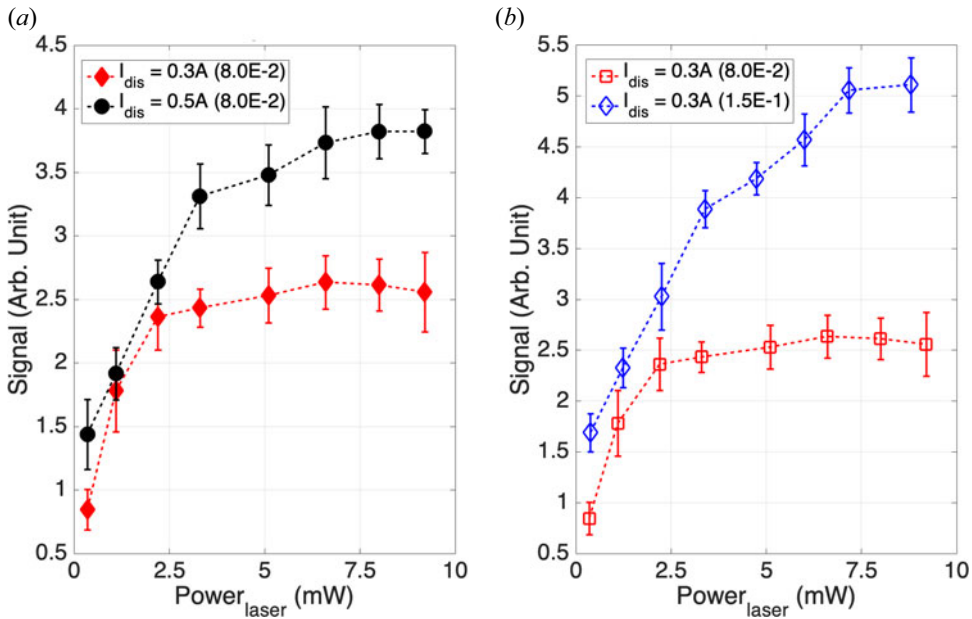


FIGURE 4. Changing laser power under different plasma discharge current (*a*) and different neutral pressure (*b*) to explore the output limit of fluorescence. The red diamond and the black circle represent discharge currents of 0.3 and 0.5 A, respectively (*a*). The blue diamond and red square represent the fluorescence signal intensity at neutral pressures of 1.5×10^{-1} and 8.0×10^{-2} Pa, respectively, while keeping the discharge current constant at 0.3 A (*b*).

is set to 10 s and the time constant is 30 ms. The recovered LIF signal is averaged over 32 scans. All data are collected using an oscilloscope.

5. Experimental results and discussion

According to the collision model of metastable ion generation, fluorescence frequency can be changed by changing the production rate of metastable ions. This can in turn be done by, for example, changing the plasma discharge current or the neutral pressure, which changes the number of energetic electrons and neutrals from which metastable ions are produced. Two experiments of different discharge current are designed, as shown in figure 4. The electron temperature and electron density are measured by a Langmuir probe. The data are shown in table 1. The neutral pressure is controlled by the flowmeter and detected as 8.0×10^{-2} Pa by the vacuum gauge. Figure 4(*a*) demonstrates that, for the same laser power injection, higher discharge currents result in higher fluorescence signals and their limit. In this work, all recorded signals are normalized by the sensitivity of the lock-in amplifier, and the sensitivity of the PMT stayed constant. Increasing the discharge current from 0.3 to 0.5 A gives an increased fluorescence signal by a factor of 1.46, which is significantly lower than the 1.67 ratio of discharge current increase. This may be due to the partial loss of the initial high-energy electrons produced by the hot cathode at low neutral pressure. Table 1 also shows that changing the discharge current does not significantly change T_e , but changing the neutral pressure does significantly change both n_e and T_e . This is expected as in a weakly ionized plasma, i.e. $n_e \ll n_n$, where n_n is the neutral density, energy dissipation of the energetic electrons is generally determined by electron loss to the wall and collisional loss to the background neutrals, both of which are

Discharge current (A)	Neutral particle pressure (Pa)	Electron density (cm ⁻³)	Electron temperature (eV)
0.3	8.0×10^{-2}	1.09×10^9	4.41
0.5	8.0×10^{-2}	1.75×10^9	4.46
0.3	1.5×10^{-1}	4.78×10^9	2.84

TABLE 1. Electron temperature and electron density data measured by a Langmuir probe under three different conditions.

relatively constant parameters with respect to discharge power unless a plasma is close to being fully ionized.

In the case of two different discharge currents, the intensity growth rate of fluorescence signal decreases with an increase of laser power. It can also be seen from [figure 4\(a\)](#) that at higher discharge current, the laser power needs to be higher to reach the fluorescence intensity limit. This is because a higher discharge current provides more energetic electrons, increasing the production rate of metastable ions.

The neutral pressure in the chamber can be accurately controlled by the gas flowmeter. Therefore, an experiment to study the generation limit of fluorescence signal under different neutral pressures was also designed. The experimental results are shown in [figure 4\(b\)](#). As shown, the proportional increase of LIF signal with an increase of neutral pressure is higher than that with an increase of discharge current. This is consistent with the results that a higher discharge current at a lower neutral pressure facilitates higher loss of primary electrons to the wall than to the collisions with neutral gas, and also consistent with results of previous studies that electron–neutral collisions produce both ground-state ions and metastable ions.

When the plasma parameters remain constant, the yield of metastable ions per unit time, i.e. the rate of metastable ion production, is limited. This in turn limits the excitation frequency of LIF for the same laser power. From [figure 4](#), we can also obtain the laser power saturation under the three different conditions in [table 1](#): 2.5 mW (0.3 A, 8.0×10^{-2} Pa), 6.2 mW (0.5 A, 8.0×10^{-2} Pa) and 7.5 mW (0.3 A, 1.5×10^{-1} Pa), the parameters in parentheses representing discharge current and neutral particle pressure, respectively. Below we present results of exploring the frequency limit of fluorescence signal output, with the frequency modulation realized by AOM modulation of a continuous-wave laser.

The frequency limit of fluorescence output under changing discharge current and neutral pressure was also studied in this paper. In this series of experiments, the laser injection was kept unchanged at a low power (1.48 mW). It is worth noting that we used the function of automatic phase finding of the lock-in amplification before each experiment to avoid an excessive phase difference between the lock-in amplification and AOM, especially in the high-laser-chopping-frequency experiment, where the method of increasing the plasma discharge current and then accurately finding the phase is used. The results are shown in [figure 5](#). The signal strength here indicates the integral value of the whole ion velocity distribution function signal strength under a Maxwell distribution to avoid the impact of noise signal on the peak value of the fluorescence signal. The effect of discharge current on fluorescence limit frequency is investigated first. The results are shown in [figure 5\(a\)](#). The four groups maintained the same neutral pressure and iris size. The fluorescence signal declines much more rapidly after the frequency with maximum signal is reached, as shown in [figure 5\(a\)](#), especially when the plasma discharge current

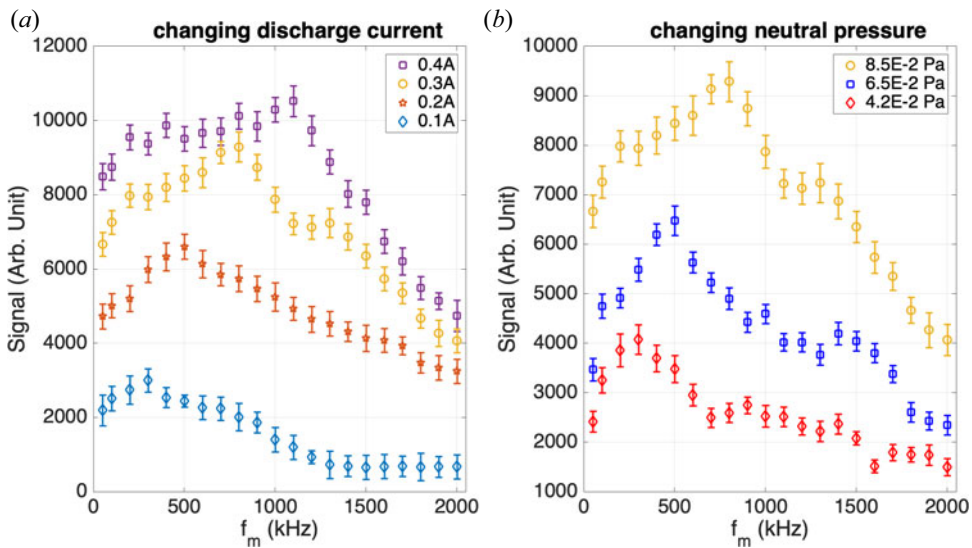


FIGURE 5. Exploring the frequency limit of fluorescence output under changing discharge current with the neutral pressure kept constant at 8.5×10^{-2} Pa (a) and changing neutral pressure with a discharge current of 0.3 A (b).

is high. This is consistent with the collision excitation model for which an increased rate of primary electron injection increases the metastable production rate, which increases the fluorescence frequency. Before reaching the extreme value, the fluorescence signal intensity increases with an increase of laser input frequency, reflecting suppression of lower-frequency noise. The lower frequency mostly refers to the noise produced by the circuit. This noise has a broad spectrum of frequencies, and the frequency ranges could be composed of a Fourier expansion with the same frequency as the lock-in amplification. When the chopping frequency exceeds the broad-spectrum noise frequency ranges (which are often less than 200 kHz), this noise could be suppressed, resulting in an increase in signal strength. The shift to higher frequency with maximum signal strength at a higher discharge current and laser power indicates the association of such frequency with the fluorescence excitation frequency in the diagnosed volume, and that the background noise is broadband such that increasing modulation frequency removes an increasing portion of the frequency components of these noises. Once a maximum frequency is reached, the signal begins to decline with further increase of modulation frequency. It is worth noting that the decreasing amplitude of the signal will gradually decrease with a gradual increase of the chopper frequency. At the same time, this trend is also seen in the experiment of changing the neutral pressure in figure 5(b). With the modulated real signal not expected to be removed by lock-in amplification, this reduction of signal is therefore an evidence of frequency decoupling between the laser modulation and the waveform of the fluorescence signal.

As listed in table 2, under these different sets of discharge parameters, several turning fluorescence frequencies were observed. Turning frequency here represents the extreme frequency observed experimentally. Meanwhile, the fluorescence frequency in table 2 represents the extreme frequency calculated by PMT gain. The fluorescence frequency can be calculated by converting the observed signal to the actual photon count via the PMT's luminous sensitivity. The PMT voltage signal is converted to light intensity in

Case	Electron density (cm^{-3})	Electron temperature (eV)	Turning frequency with lock-in amplification (kHz)	Fluorescence frequency measured by PMT (MHz)
1 (0.1 A, 8.5×10^{-2} Pa)	6.45×10^8	4.63	300	3.15
2 (0.2 A, 8.5×10^{-2} Pa)	1.23×10^9	4.81	500	6.81
3 (0.3A, 8.5×10^{-2} Pa)	1.89×10^9	4.65	800	9.54
4 (0.4A, 8.5×10^{-2} Pa)	2.64×10^9	4.72	1100	11.40
5 (0.3 A, 6.5×10^{-2} Pa)	1.39×10^9	5.22	500	6.74
6 (0.3A, 4.2×10^{-2} Pa)	1.07×10^9	5.53	300	4.14

TABLE 2. The turning frequency with lock-in amplification and the fluorescence frequency estimated by the photon count under the corresponding experimental conditions obtained by PMT gain conversion. (Case1: discharge current 0.1 A, 8.5×10^{-2} Pa; case2: discharge current 0.2 A, 8.5×10^{-2} Pa; case 3: discharge current 0.3 A, 8.5×10^{-2} Pa; case 4: discharge current 0.4 A, 8.5×10^{-2} Pa; case 5: discharge current 0.3 A, 6.5×10^{-2} Pa; case 6: discharge current 0.3 A, 4.2×10^{-2} Pa; all cases used the same laser power of 1.48 mW.) In addition, the electron temperature and density measured by a Langmuir probe are also shown.

luminous units using the specified lumens-to-voltage sensitivity of the PMT provided by its manufacturer's test report, which is then converted to power units (watts) and thence the photon count using the photon energy of the fluorescent light calculated by $E = h\nu$. The calculated fluorescence frequencies are much higher than the turning frequency observed in the experiment. We believe that the optimal modulation frequency being at most 1/10 of the fluorescence frequency is specific to analogue lock-in amplification and is not generally applicable if signal amplification techniques are different. This is because the real frequency of the probabilistic signal becomes decoupled from the modulation frequency and analogue-based lock-in amplification is, obviously, particularly sensitive to the coupling of the reference frequency and the signal modulation frequency. On the other hand, the reduction of signal strength is found to be a very gradual process. This indicates the lack of a rapid transition from a statistically determined signal to a probabilistically determined signal, with which the whole signal should be removed by lock-in amplification. Rather, such a transition is a gradual process, with the total photon count per laser pulse becoming partially probabilistic, and lock-in amplification clips away the random 'portion' of the signal. That is, the gradual manifestation of the probabilistic nature of fluorescence photon counting is more like the case shown in figure 1(b) instead of a rapid transition to zero recovered signal, as with the case shown in figure 1(a). Note that the PMT is also not a single-photon detector, which might add to this effect. Therefore, this process needs to be considered when using the locked-in amplifier to extract the weak signal in the LIF experiment, and because the measured fluorescence signal generation frequency is far less than the theoretically calculated fluorescence frequency, this will bring restrictions in instability and other plasma high-frequency oscillation experiments.

6. Conclusion

A series of experiments in LTS were conducted to explore the generation limit of fluorescence signal. By changing the plasma discharge current and neutral pressure to control the number of metastable states in the device, it is found that under the

same laser power injection, the fluorescence signal increases with the increase of metastable states in the device, and the fluorescence frequency also increases. With a fixed fluorescence frequency, increasing the laser modulation frequency first increases the signal as lower-frequency noise is being removed, until a maximum signal is reached. Beyond this characteristic frequency, increasing the modulation frequency gradually reduces the observed signal. This reflects a transition from the statistically determined macroscopic signal, which is very stable from pulse to pulse, to the microscopic, probabilistic nature of laser-excited fluorescence as the modulation frequency, and that the lock-in application process has removed the resultant fluctuating signal. In essence, increasing the modulation frequency is equivalent to reducing the event count per laser pulse and is thus a transition from a macroscopic experiment to a microscopic experiment, and we have shown that such a transition indeed occurs and is a gradual process. Thus, when an LIF diagnostics is designed, it is advised that one considers such an effect when determining the modulation frequency. In addition, available evidence suggests that the signal reduction effect is also associated with lock-in amplification as the modulation frequency and the real signal frequency become decoupled. If other means of signal recovery are employed, like an up/down counting technique (Mattingly & Skiff 2018; Hood *et al.* 2020), the results might be very different.

Acknowledgement

The authors would like to express their grateful acknowledgement in memory of the late Dr Noah Hershkowitz, Irving Langmuir Professor Emeritus of the University of Wisconsin-Madison, and a long-time collaborator of the authors, who has given invaluable advice and discussions concerning our studies associated with sheath/presheath and diagnostics-associated physics.

Funding

This work is supported by the National Natural Science Foundation of China (contract no. 11875285), the President Funding of Hefei Institutes of Physical Science, Chinese Academy of Sciences (YZJJ2022QN19), the CAS Key Research Program of Frontier Sciences (grant no. QYZDB-SSW-SLH001) and the Chinese Academy of Science Hundred Youth Talent Program.

Declaration of interests

The authors report no conflict of interest.

Data availability statement

The data that support the findings of this study are available from the corresponding author upon reasonable request.

Author contributions

D.J.: Writing – review and editing, Writing – original draft, Investigation, Formal analysis, Data curation. C.-y.J.: Methodology, Conceptualization. C.-S.Y.: Funding acquisition, Project administration, Resources, Supervision. W.Z.: Data curation and analysis. G.-S.X.: Resources, Supervision. L.W.: Resources, Supervision.

REFERENCES

BARNAT, E.V. & WEATHERFORD, B.R. 2015 2D laser-collision induced fluorescence in low-pressure argon discharges. *Plasma Sources Sci. Technol.* **24**, 055024.

- BOIVIN, R.F. & SCIME, E.E. 2003 Laser induced fluorescence in Ar and He plasmas with a tunable diode laser. *Rev. Sci. Instrum.* **74**, 4352–4360.
- CHU, F., HOOD, R. & SKIFF, F. 2019 Measurement of wave-particle interaction and metastable lifetime using laser-induced fluorescence. *Phys. Plasmas* **26**, 042111.
- CHU, F., MATTINGLY, S.W., BERUMEN, J., HOOD, R. & SKIFF, F. 2017 On determining the fraction of metastable ions produced by direct ionization. *J. Instrum.* **12**, C11005–C11005.
- CHU, F. & SKIFF, F. 2018 A Lagrangian model for laser-induced fluorescence and its application to measurements of plasma ion temperature and electrostatic waves. *Phys. Plasmas* **25**, 013506.
- COOPER, C.S. & LAURENDEAU, N.M. 1997 Effect of pulsed dye-laser wavelength stabilization on spectral overlap in atmospheric NO fluorescence studies. *Appl. Opt.* **36**, 5262–5265.
- DUAN, X., CHENG, M., YANG, X., GUO, N., LI, X., WANG, M. & GUO, D. 2020 Investigation on ion behavior in magnetically shielded and unshielded Hall thrusters by laser-induced fluorescence. *J. Appl. Phys.* **127**, 093301.
- HOOD, R., BAALRUD, S.D., MERLINO, R.L. & SKIFF, F. 2020 Laser-induced fluorescence measurements of ion fluctuations in electron and ion presheaths. *Phys. Plasmas* **27**, 053509.
- JACOBS, B., GEKELMAN, W., PRIBYL, P., BARNES, M. & KILGORE, M. 2007 Laser-induced fluorescence measurements in an inductively coupled plasma reactor. *Appl. Phys. Lett.* **91**, 161505.
- KEESEE, A.M., SCIME, E.E. & BOIVIN, R.F. 2004 Laser-induced fluorescence measurements of three plasma species with a tunable diode laser. *Rev. Sci. Instrum.* **75**, 4091–4093.
- LEE, D., HERSHKOWITZ, N. & SEVERN, G.D. 2007a Measurements of Ar⁺ and Xe⁺ velocities near the sheath boundary of Ar–Xe plasma using two diode lasers. *Appl. Phys. Lett.* **91**, 041505.
- LEE, D., OKSUZ, L. & HERSHKOWITZ, N. 2007b Exact solution for the generalized Bohm criterion in a two-ion-species plasma. *Phys. Rev. Lett.* **99**, 155004.
- LEE, D., SEVERN, G., OKSUZ, L. & HERSHKOWITZ, N. 2006 Laser-induced fluorescence measurements of argon ion velocities near the sheath boundary of an argon–xenon plasma. *J. Phys. D: Appl. Phys.* **39**, 5230–5235.
- MATTINGLY, S.W. & SKIFF, F. 2018 FPGA based demodulation of laser induced fluorescence in plasmas. *Rev. Sci. Instrum.* **89**, 043508.
- MAZOUFFRE, S. 2012 Laser-induced fluorescence diagnostics of the cross-field discharge of Hall thrusters. *Plasma Sources Sci. Technol.* **22**, 013001.
- MAZOUFFRE, S., GAWRON, D., KULAEV, V. & SADEGHI, N. 2008 Xe⁺ ion transport in the crossed-field discharge of a 5-kW-class hall effect thruster. *IEEE Trans. Plasma Sci.* **36**, 1967–1976.
- MOORE, N.B., GEKELMAN, W. & PRIBYL, P. 2016 Ion energy distribution function measurements by laser-induced fluorescence in a dual radio frequency sheath. *J. Vac. Sci. Technol. A* **34**, 021303.
- ROMADANOV, I., RAITSES, Y., DIALLO, A., HARA, K., KAGANOVICH, I.D. & SMOLYAKOV, A. 2018 On limitations of laser-induced fluorescence diagnostics for xenon ion velocity distribution function measurements in Hall thrusters. *Phys. Plasmas* **25**, 033501.
- SEVERN, G.D., EDRICH, D.A. & MCWILLIAMS, R. 1998 Argon ion laser-induced fluorescence with diode lasers. *Rev. Sci. Instrum.* **69**, 10–15.
- SEVERN, G., LEE, D. & HERSHKOWITZ, N. 2007 Xenon ion laser-induced fluorescence using a visible tunable diode laser near 680 nm. *Rev. Sci. Instrum.* **78**, 116105.
- SUN, X., COHEN, S.A., SCIME, E.E. & MIAH, M. 2005 On-axis parallel ion speeds near mechanical and magnetic apertures in a helicon plasma device. *Phys. Plasmas* **12**, 103509.
- WANG, X. & HERSHKOWITZ, N. 2006 Experimental studies of the two-ion species flow in the plasma presheath. *Phys. Plasmas* **13**, 053503.
- WILSON, J.M., FINN, N., JAMES, B.W. & FALCONER, I.S. 1995 A comparison of laser-induced fluorescence measurements in hydrogen with collisional radiative model calculations. *J. Phys. B: Atom. Mol. Opt. Phys.* **28**, 765–772.
- YIP, C.-S., HERSHKOWITZ, N., SEVERN, G. & BAALRUD, S.D. 2016 Laser-induced fluorescence measurements of argon and xenon ion velocities near the sheath boundary in 3 ion species plasmas. *Phys. Plasmas* **23**, 050703.
- YIP, C.S., HERSHKOWITZ, N. & SEVERN, G. 2010 Experimental test of instability-enhanced collisional friction for determining ion loss in two ion species plasmas. *Phys. Rev. Lett.* **104**, 225003.

- YIP, C.S. & JIANG, D. 2021 Laser induced fluorescence diagnostic for velocity distribution functions: applications, physics, methods and developments. *Plasma Sci. Technol.* **23**, 055501.
- ZIMMERMAN, D.C., MCWILLIAMS, R. & EDRICH, D.A. 2005 Two-dimensional ion velocity distribution functions in inductively coupled argon plasma. *Plasma Sources Sci. Technol.* **14**, 581–588.